# Hysteresis in phase volumes, compositions and interfacial roughness in model OPV-small-molecule/polymer thin-films

## Supporting Information

### Supporting information for figure 2;

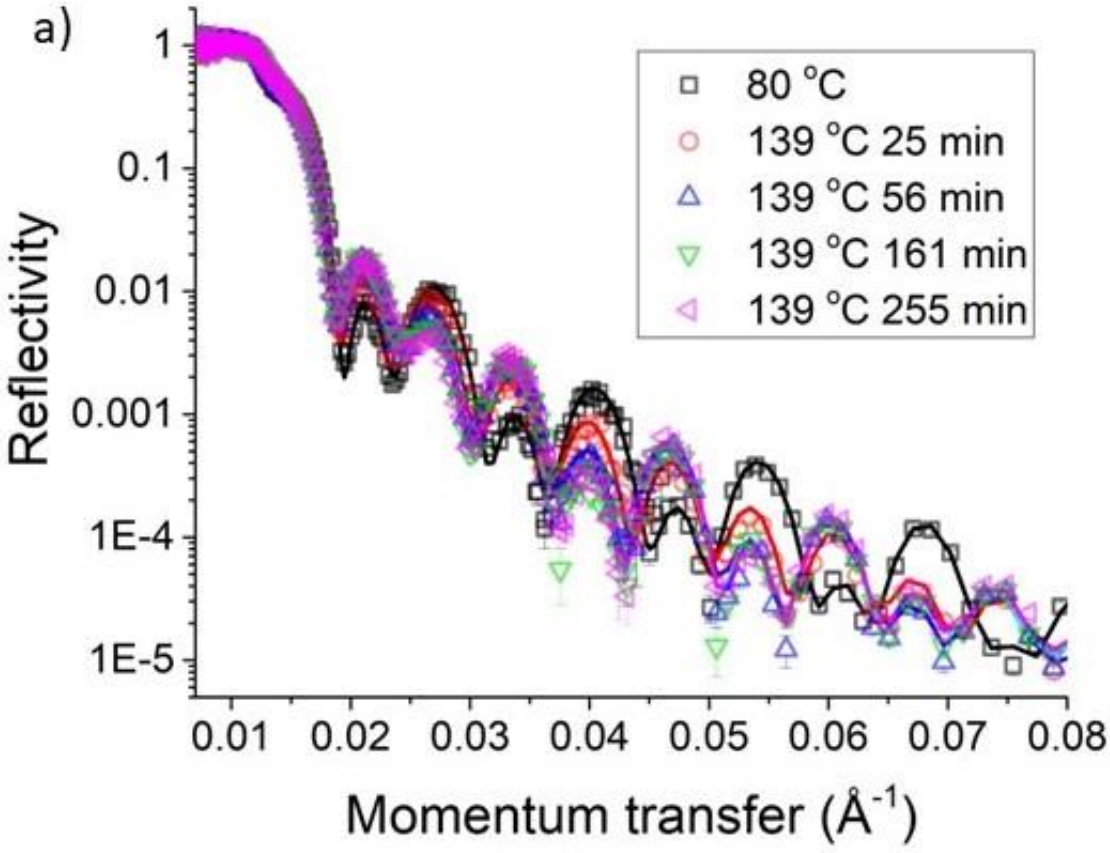


**Figure S2_1; NR curves and (unconstrained) fits for sample D at various times during isothermal annealing.** This shows the same data and fits as in figure 2, but without the curves being offset vertically. Constrained fits of these data are shown in figure S5_4.

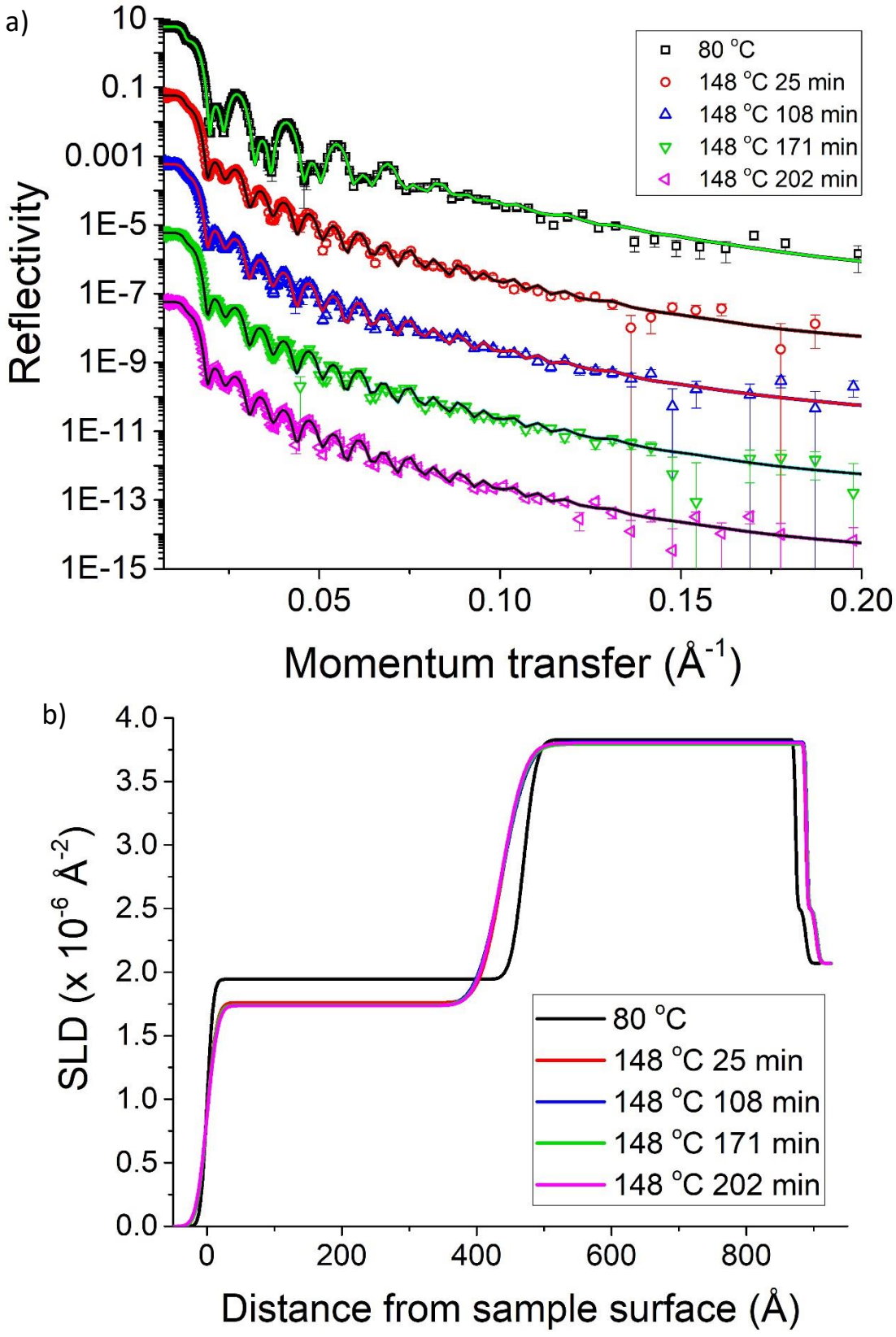


**Figure S2_2; a) NR curves and (unconstrained) fits, and b) SLD profiles, for sample E at various times during isothermal annealing.**

## Supporting information for figure 4;

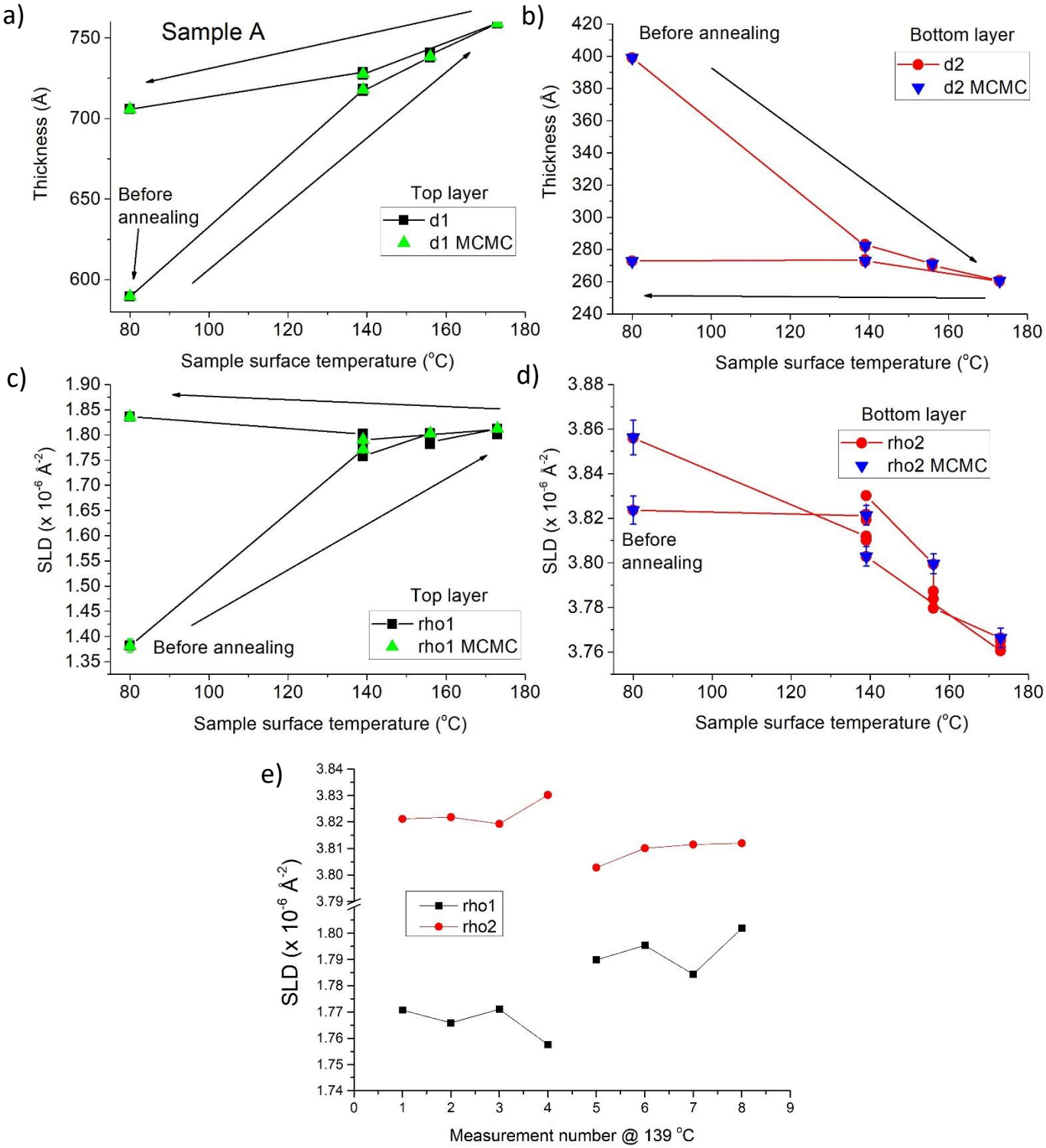


**Figure S4_1; Unconstrained fit parameters for sample A (300k PS top layer initially); a)** and **b)** show layer thicknesses, and **c)**, **d)** and **e)** show layer scattering length densities (SLDs). As well as the standard Levenberg-Marquardt/differential evolution algorithm, some fit parameters (and their uncertainties) from a Markov-chain-Monte-Carlo (MCMC) algorithm are shown. Where the MCMC fit parameter error bars can't be seen, they are smaller than the symbols (see figures S8_1 to S8_4 and table S4 for further details regarding MCMC). In addition, MCMC fit parameters and their uncertainties can also be found (for samples D and E) in Higgins et al.[1] Figure e) re-plots the SLD parameters (from the Levenberg-Marquardt fits only) in c) and d) at 139 °C; measurements 1-4 are on first heating to 139 °C, and measurements 5-8 are at 139 °C after going to higher temperatures. These fits accompany those for sample A in figures 4a and 4c.

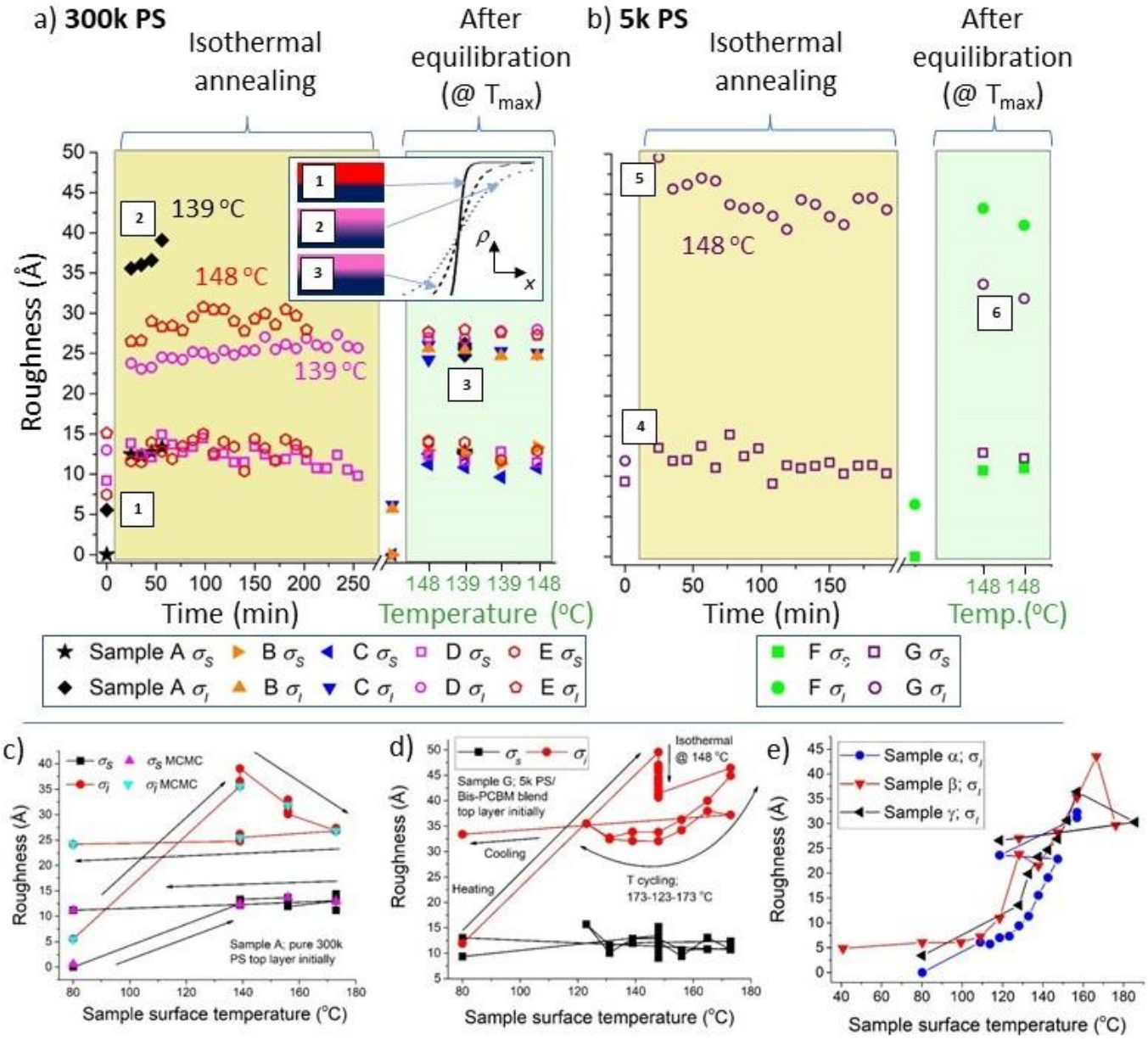


**Figure S4_2;** a) to d) reproduce the interfacial roughness data from figures 4 a) to d), with the addition of the surface roughness parameters, $\sigma_s$. The data from figures 4c) to 4e) is reproduced in figures c), d) and e) respectively, along with some additional details. In c), d) and e) the points are joined by lines in chronological order of the NR measurements. In c) as well as the standard Levenberg-Marquardt/differential evolution algorithm, some fit parameters from a Markov-chain-Monte-Carlo (MCMC) algorithm are shown. The MCMC fit parameter error bars are smaller than the symbols (see figures S11 to S11_4 and table S4 for further details regarding MCMC). In e) $\sigma_i$ measurements from an additional sample (sample $\alpha$) from batch B are also shown.

**Interfacial roughness measurements in specular NR**

The roughness measured by NR at a liquid-liquid interface is in general a combination of molecular mixing of the components and lateral roughness.[2,3] In an equilibrated liquid–liquid system the so-called 'intrinsic width', that characterises the molecular mixing, will depend on the chemical compatibility of the component molecules and the MW of any polymeric constituents, while lateral roughness will occur via thermally-activated capillary-waves.[4,5] Thermal capillary-waves show an increase in amplitude with wavelength.[3] and, given sufficient contrast across the

interface, would be expected to give rise to off-specular scattering within the in-plane *q* range (corresponding to in-plane distances of a few hundred nanometres to a few micrometres) accessible on D17.[2]

The detector maps in figure S4_3 and S4_4 show little evidence of any of the off-specular scattering that would be expected to occur if the samples contained significant lateral roughness (at the buried interface, the substrate or the sample surface). Detailed investigations of off-specular scattering usually involve significantly longer measurement times than typically used in specular reflectometry experiments.[2] To compensate for this we have summed the detector maps for four consecutive NR measurements during in-situ annealing at elevated temperature for samples A and G (figures S4_3 c) and d) and S4_4 c) and d)). Projections of these maps onto the x-axis (corresponding to the scattering angle of the neutrons) are shown in figure S4_5 in comparison with projections for the samples at 80 °C (with the latter scaled by a factor of 4 to account for the acquisition time difference). While it is clear from these projections that the specular signal has changed following heating to elevated temperatures, there are relatively few changes away from the specular reflections (NB; the positions of the specular reflections shift slightly on the detector as a result of temperature changes). In the case of sample G (initially with a 5k PS/Bis-PCBM top layer) there is some enhanced scattering on one side of the specular reflection (between detector pixels 225 and 235) for measurements at angle 1, perhaps due to a small amount of Yoneda scattering,[2,6] that may be related to the existence of lateral morphology in the 5k PS/BisPCBM samples following annealing (see figure S9_1 d) and e) below, and figure S18 in the SI of Higgins et al.[1] However, for sample A (and for other 300 k PS samples, such as sample D, which are the main focus of our investigations) there is no change in the off-specular scattering, even in this part of the detector map, on annealing. Putting this together with evidence from optical microscopy on the 300k samples after cooling to room temperature, which shows completely uniform bilayers for the 300k PS samples (see Higgins et al,[1] figures S18 a) and b)), it is likely that the interfacial roughness parameters extracted from the specular reflectivity measurements in this study are largely due to broadening of the interface via molecular mixing.

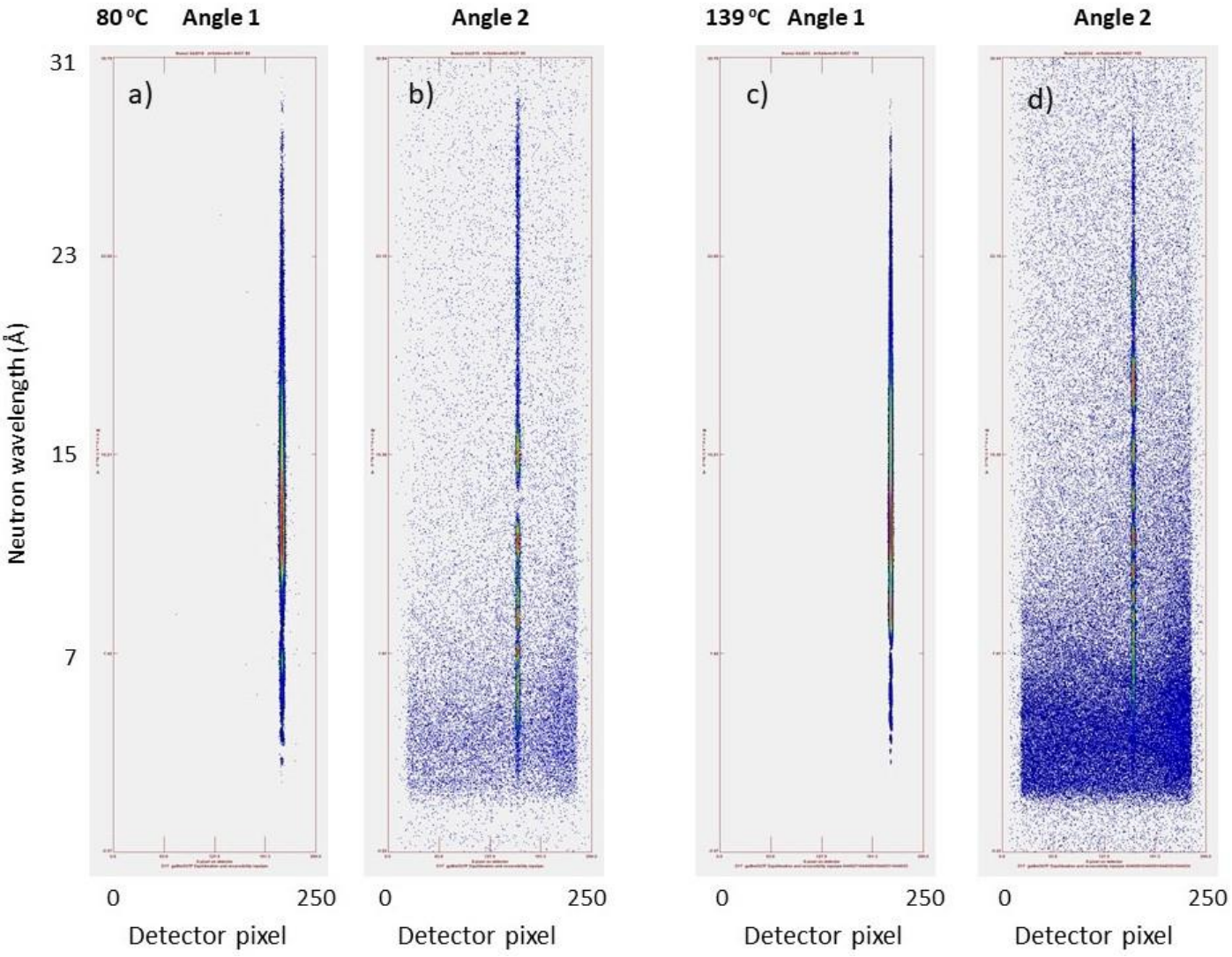

**Figure S4_3; Detector maps ('raw', neutron count data) for sample A (having a pure 300k PS top layer initially).** a) angle 1 (0.8°) and b) angle 2 (3°) at 80 °C, before annealing to higher temperature. c) angle 1 (0.8°) and d) angle 2 (3°) at 139 °C. a) and b) show single measurements (run numbers) at each angle, with 10 minutes acquisition time in total. c) and d) show the first four measurements for each angle at 139 °C added together (40 minutes acquisition time in total; 8 minutes for angle 1 and 32 minutes for angle 2). The detector pixel is related to the scattering angle of the neutrons.

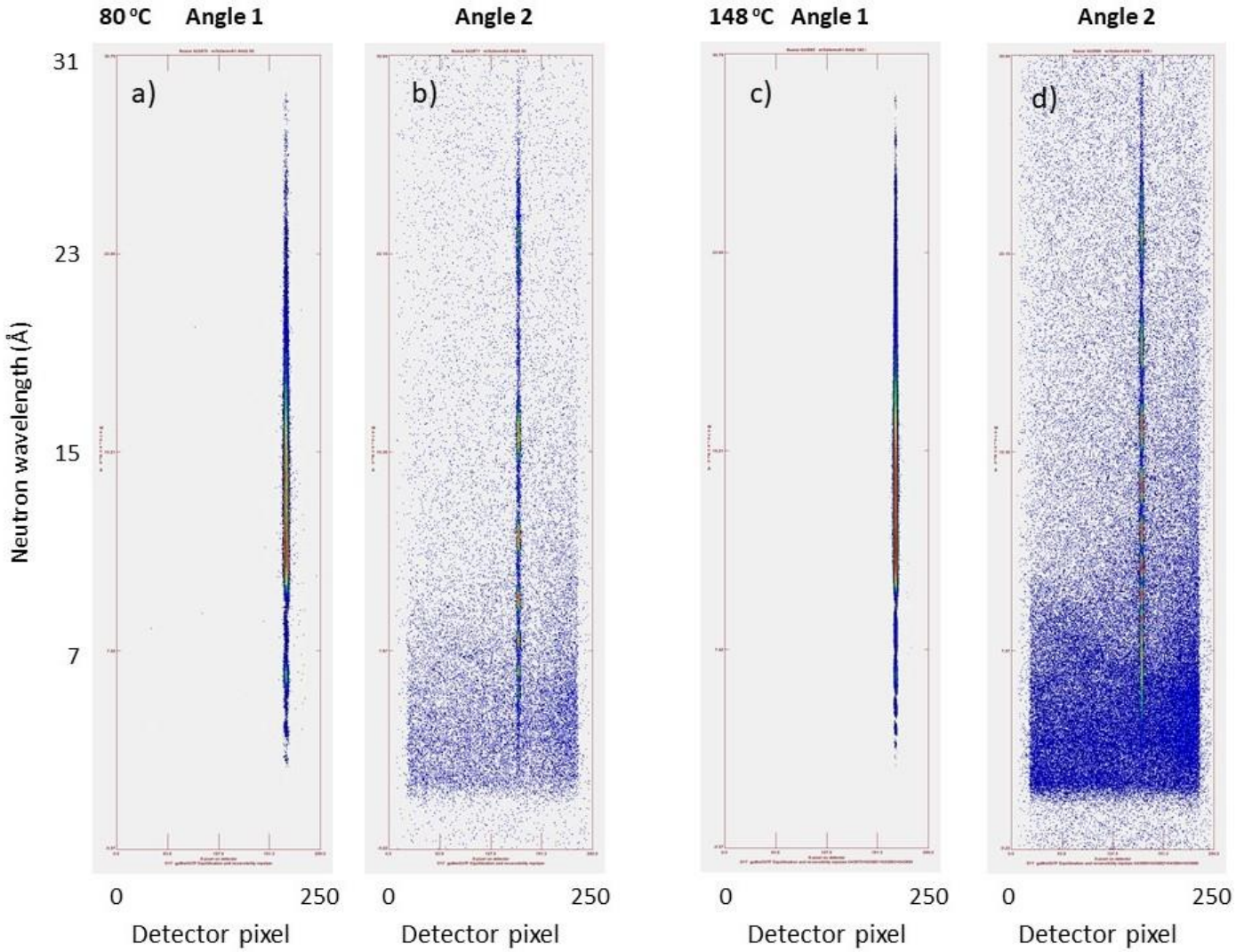


**Figure S4_4; Detector maps ('raw', neutron count data) for sample G (having a 5k PS/Bis-PCBM blend top layer initially).** a) angle 1 (0.8°) and b) angle 2 (3°) at 80 °C, before annealing to higher temperature. c) angle 1 (0.8°) and d) angle 2 (3°) at 148 °C. a) and b) show single measurements (run numbers) at each angle, with 10 minutes acquisition time in total. c) and d) show the first four measurements for each angle at 148 °C added together (40 minutes acquisition time in total; 8 minutes for angle 1 and 32 minutes for angle 2).

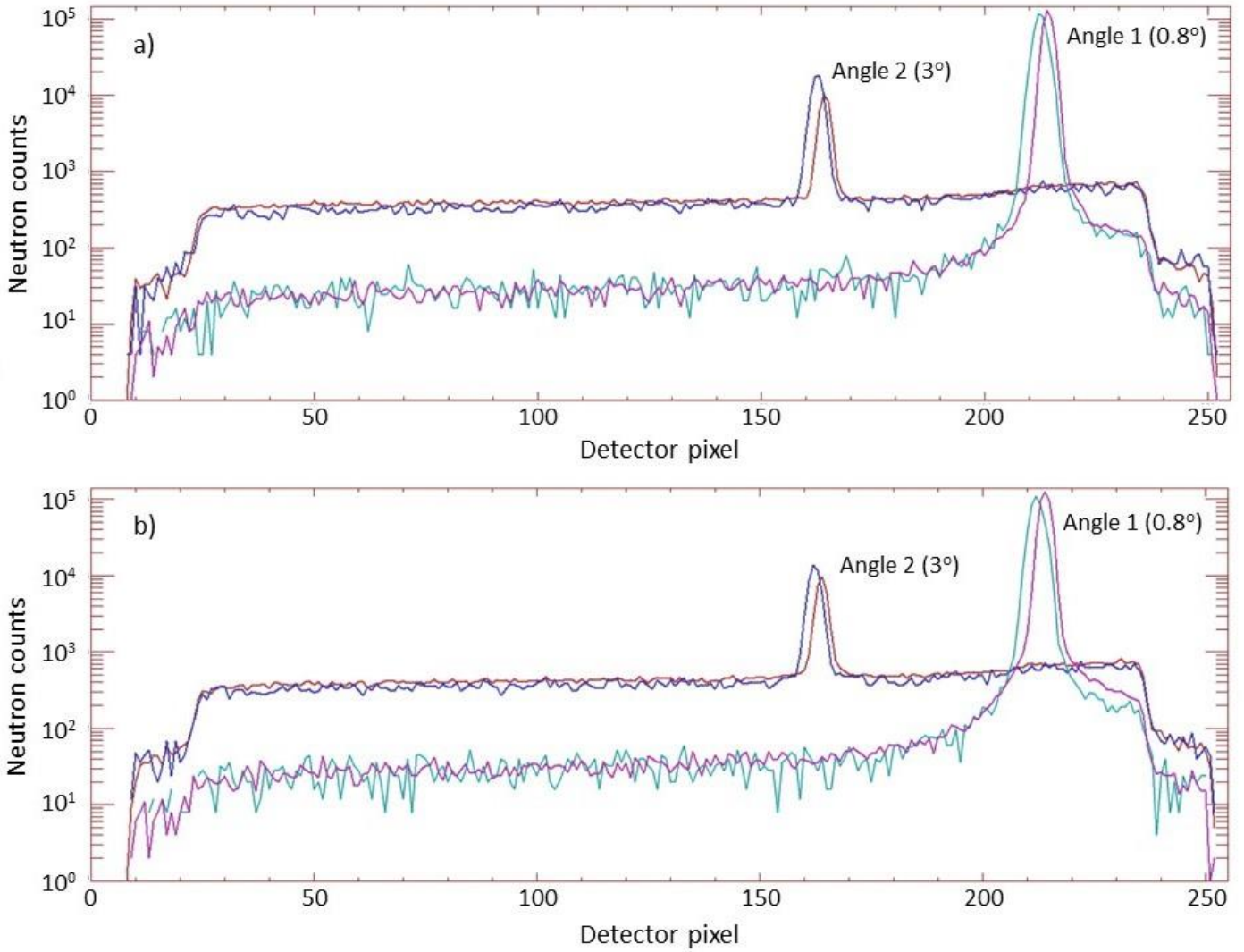


**Figure S4_5; Projections from the detector maps in S4_3 and S4_4.** a) Sample A and b) sample G. These maps show the summation of the neutron counts over the entire wavelength range shown in figures S4_3 and S4_4 projected onto the x-axes. In both a) and b) the measurements at 80 °C are shown in blue and cyan, and the measurements at 139 °C or 148 °C are shown in red and magenta. To enable comparison with the plots at the higher temperatures (which consist of four consecutive NR measurements added together), the neutron counts for the measurements at 80 °C have been multiplied by four.

## Supporting information for figure 5;

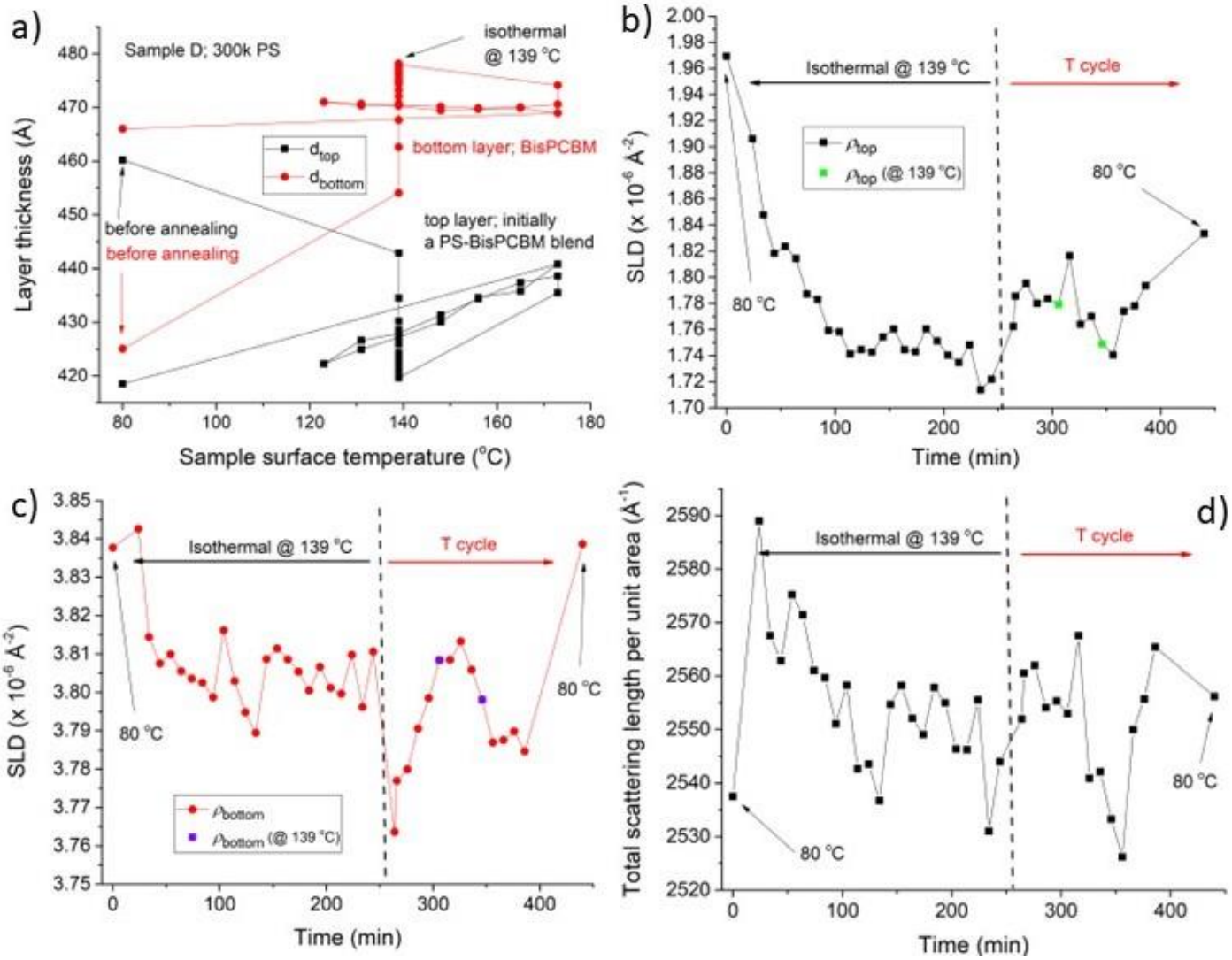


**Figure S5_1 Unconstrained fit parameters for initially 300k PS/Bis-PCBM blend top layer sample (sample D) annealed at 150 °C.** a) Layer thicknesses, b) top layer SLD, c) bottom layer SLD, and d) total scattering length per unit area, versus time. The variability in the total scattering length per unit area over time in d) gives a standard deviation that is 0.5% of the mean value. These are included for comparison with the constrained SLD fit parameters shown for this sample in figures 5c and 5d.

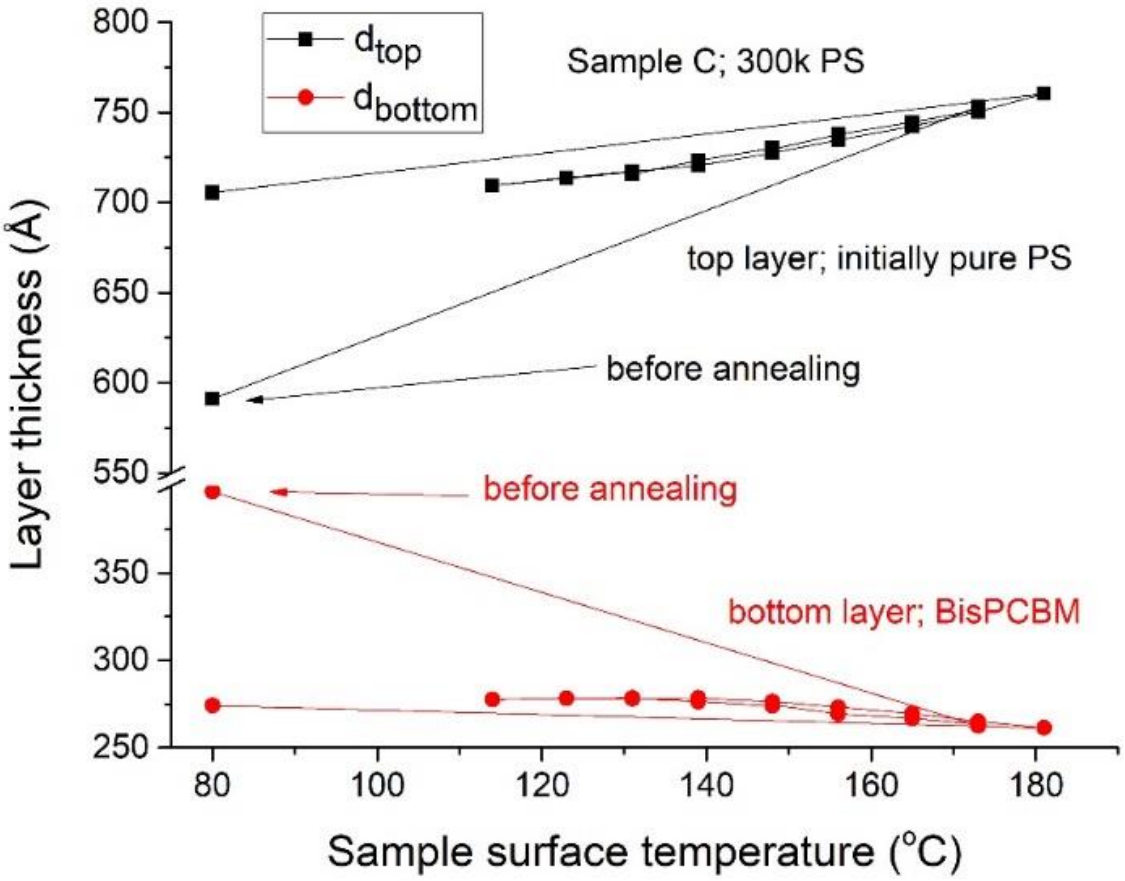


**Figure S5_2; No hysteresis after annealing at sufficiently high temperatures.** For comparison with figures 5a and 5c, this shows the evolution of layer thickness in a system that is heated straight to 173 °C prior to temperature cycling, and shows no hysteresis. This is sample C, and shows the temperature cycling data that is plotted (in a different format) in Higgins et al figures 6a and 6b,[1] plus the data at 80 °C before annealing. The fits here were unconstrained.

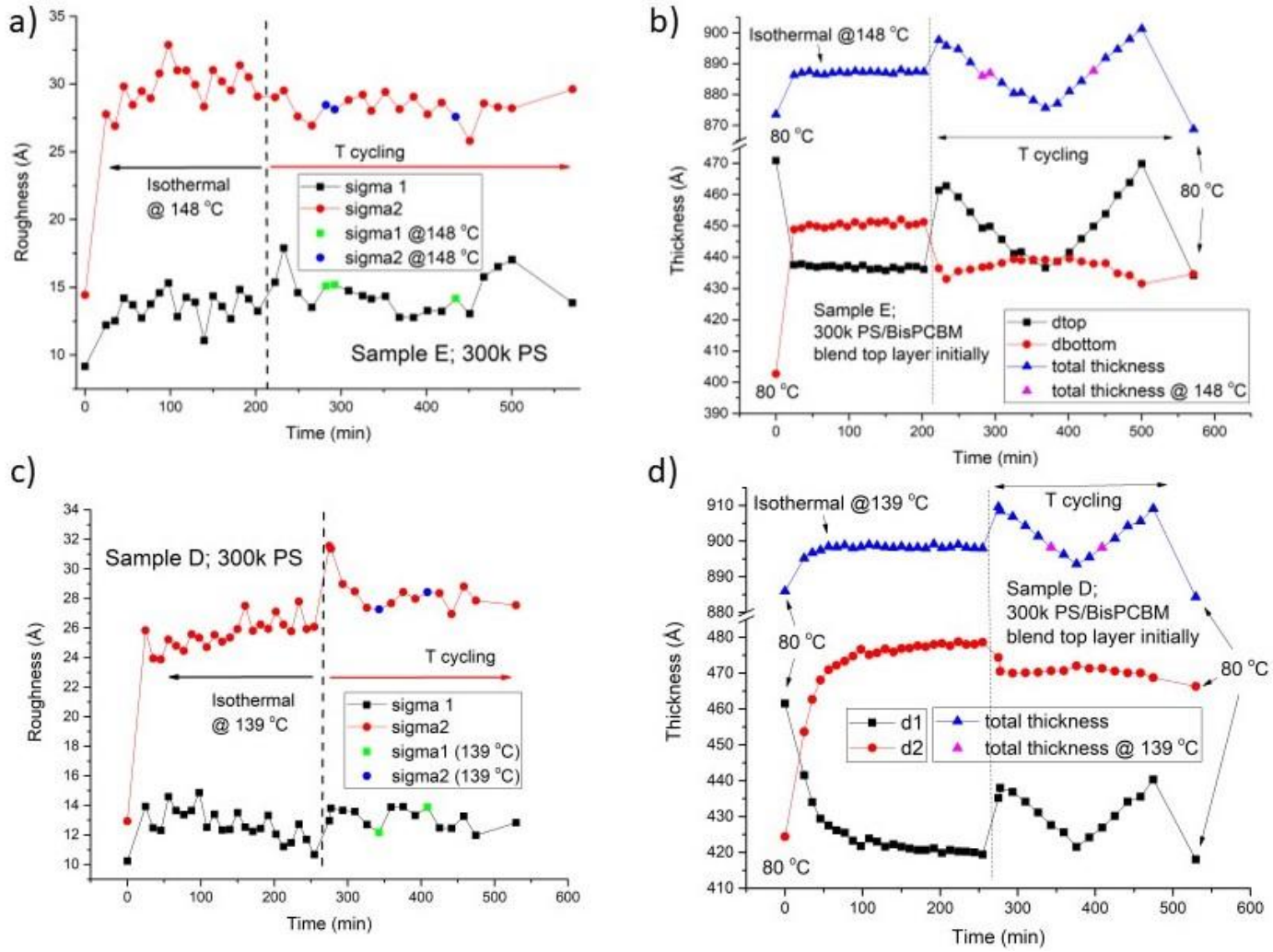


**Figure S5_3 Additional temporal plots of fit parameters to accompany figure 5 (constrained fits)**. **a)** Sample surface roughness/buried interface roughness, and **b)** layer thickness data for sample E (300k PS/Bis-PCBM blend top layer initially, annealed isothermally at 160 °C before temperature cycling). **c)** Sample surface roughness/buried interface roughness, and **d)** layer thickness data for sample D (300k PS/Bis-PCBM blend top layer initially, annealed isothermally at 150 °C before temperature cycling).

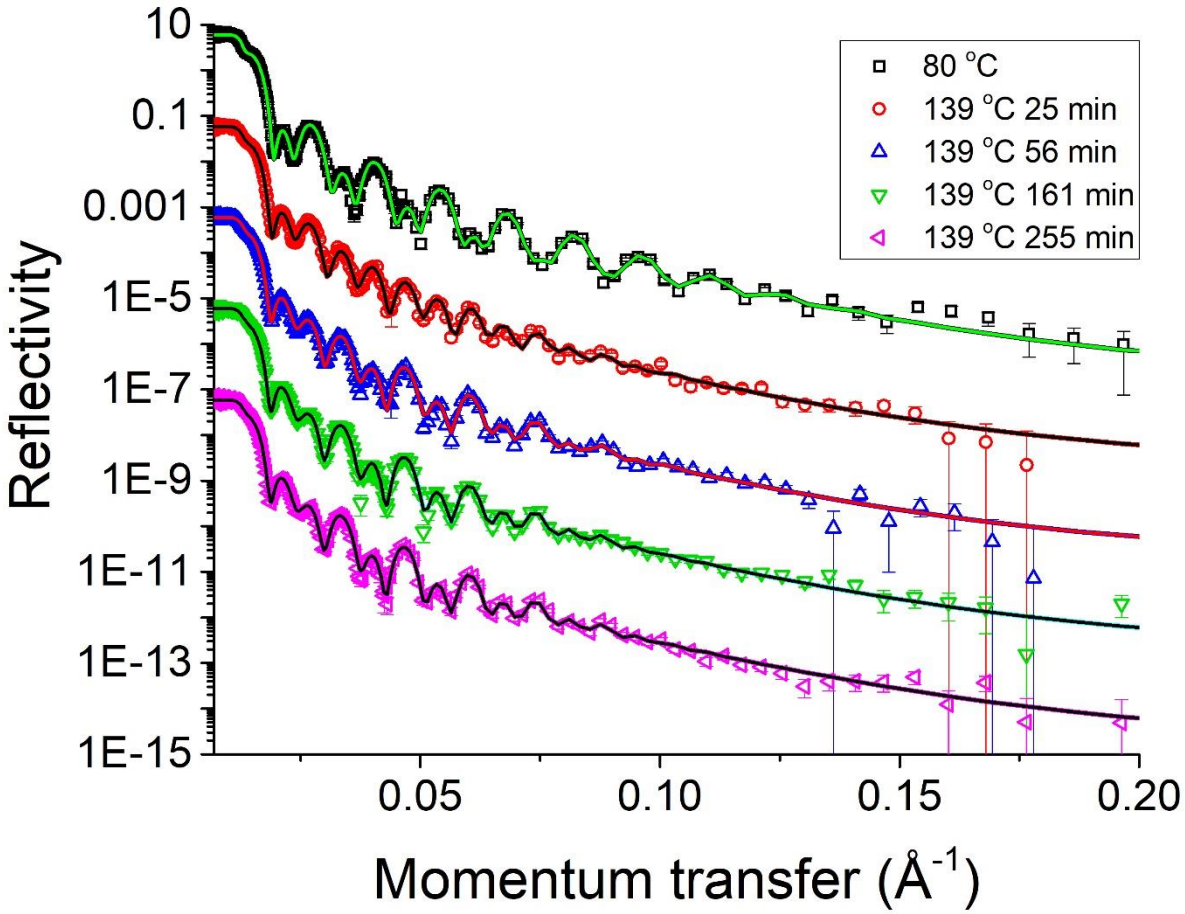


**Figure S5_4; NR curves and (*constrained*) fits for sample D at various times during isothermal annealing.** The fits are almost identical to the unconstrained fts shown in figures 2 and S2_1.

| Sample | Temperature (°C) |
|---|---|
| E (fig. 5b) | 173, 173, 165, 156, 148, 148, 139, 131, 131, 123, 114, 123, 131, 139, 148, 156, 165, 173, 181 and 80. |
| D (fig. 5d) | 173, 173, 165, 156, 148, 139, 131, 123, 131, 139, 148, 156, 165, 173 and 80. |

**Table S1; Thermal cycling temperatures in figures 5b and d;** these are the sample surface temperatures in chronological order during thermal cycling (data points with a light-green background), plus the final measurement at 80 °C.

## Supporting information for figure 7;

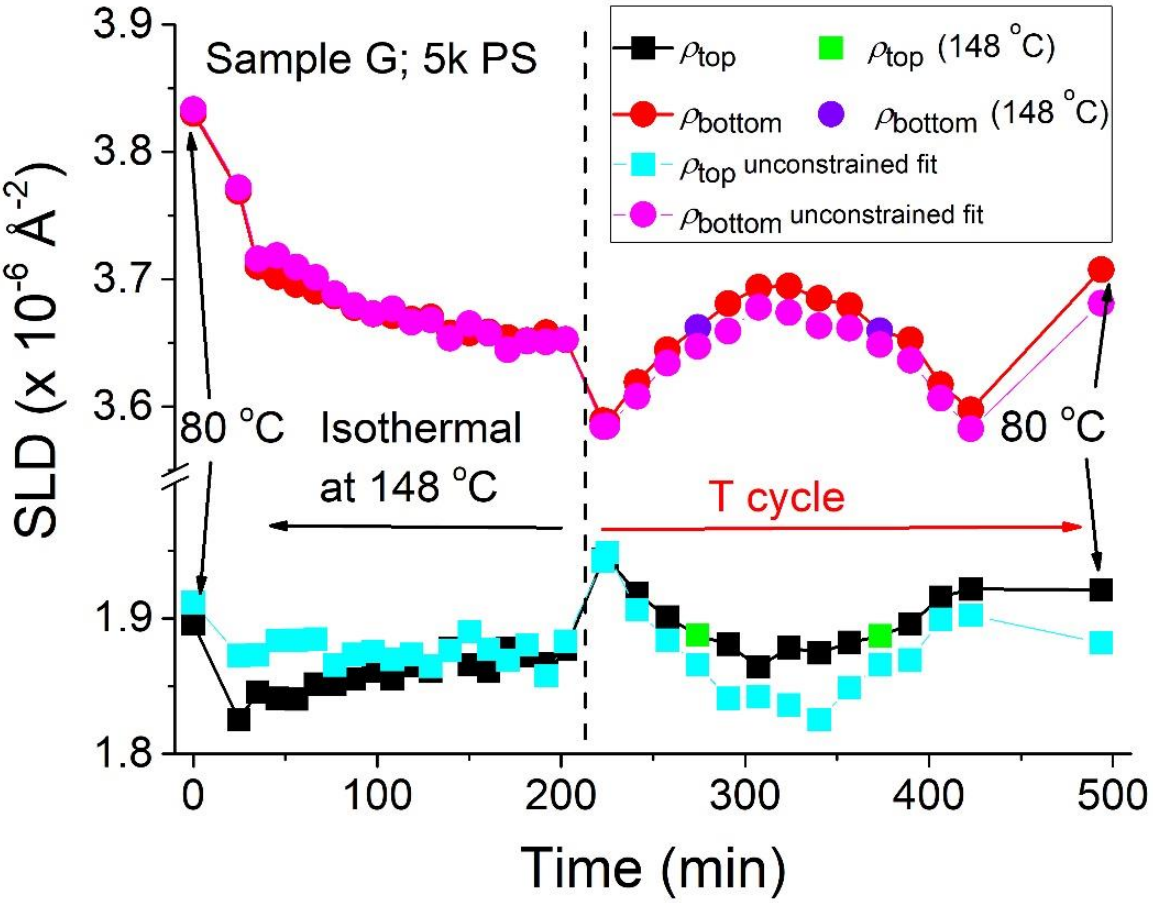


**Figure S7_1 Comparison of constrained and unconstrained fits for initially 5k PS/Bis-PCBM blend top layer sample (sample G).** This is the constrained fit parameters from fig 6c (red and black symbols), overlayed with the unconstrained fit parameters during isothermal annealing from 2c, plus the fit parameters for the constrained fits during temperature cycling on this sample.

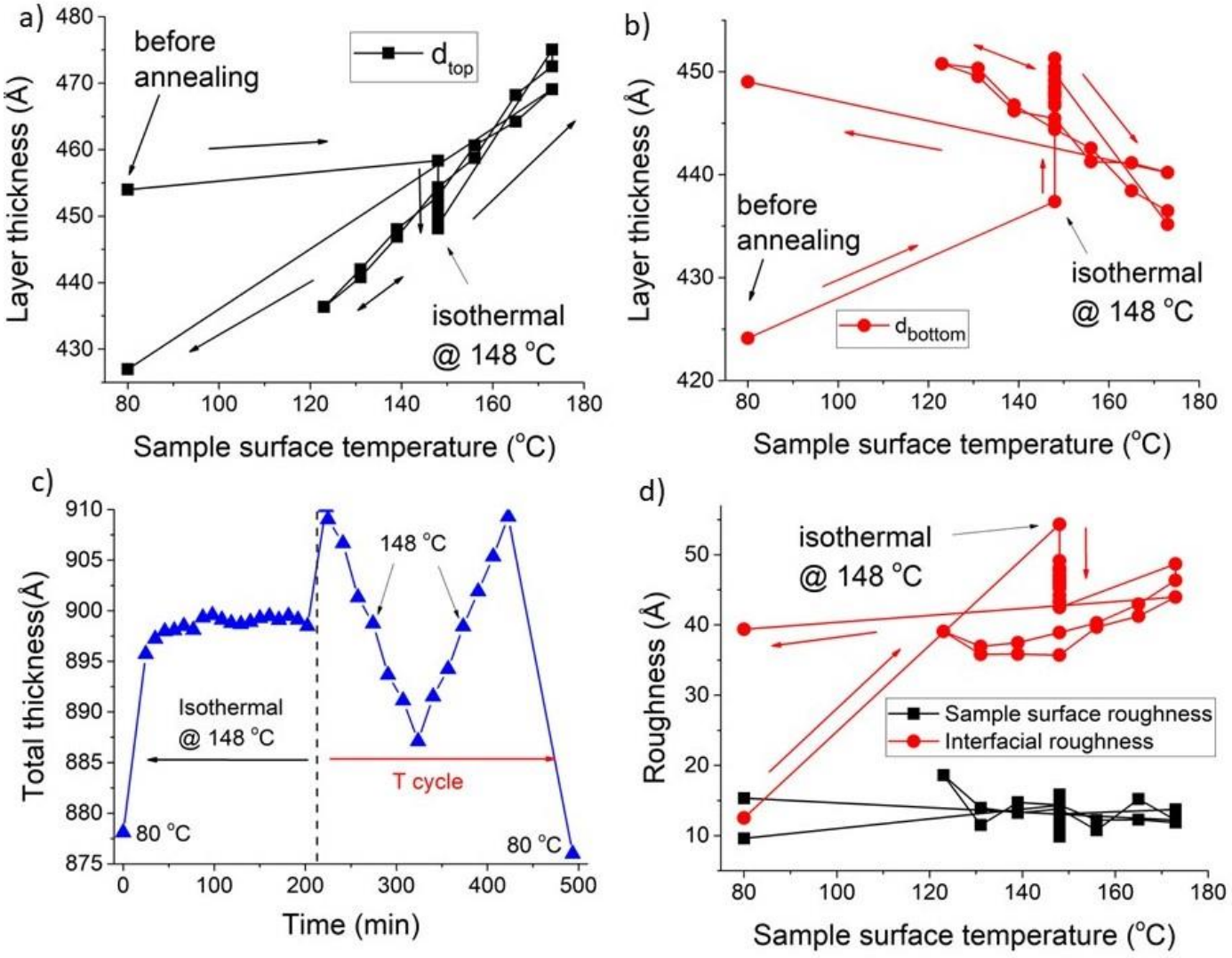


**Figure S7_2; Constrained fits for a sample that initially had a 5k PS/Bis-PCBM blend top layer (sample G; isothermal annealing at 160 °C followed by thermal cycling). a)**, **b)** Layer thickness fit parameters from figures 7a and 7b, but as a function of annealing temperature, rather than time. **c)** Total bilayer thickness as a function of time. **d)** Roughness parameters from figure 7d, but as function of annealing temperature, rather than time.

| Sample | Temperature (°C) |
|---|---|
| G (figs 7a-d) | 173, 173, 165, 156, 148, 139, 131, 123, 131, 139, 148, 156, 165, 173 and 80. |

**Table S2; Thermal cycling temperatures in figures 7a - d;** these are the sample surface temperatures in chronological order during thermal cycling (data points with a light-green background), plus the final measurement at 80 °C.

One common feature to all samples that underwent isothermal annealing followed by thermal cycling/equilibration (samples D, E and G), is the very close total volume conservation between the stabilised states during isothermal annealing and the equilibrated states at the same annealing temperatures. Figures S5_3b, S5_3d, and S7_2c show the total bilayer thicknesses for samples D, E and G. In all three samples the difference between the total bilayer thickness during isothermal annealing and at the same temperatures after equilibration is of order 0.2% or lower (in comparison to changes in the individual layer thicknesses of order 1%, and in the layer SLDs of between 0.2 and 0.5%).

# Experimental Section

## Sample preparation; further details

All samples had BisPCBM bottom layers, that were spin-coated at 2.2 x $10^3$ revolutions per minute (2.2k RPM) from chlorobenzene solutions (2.5 wt% BisPCBM). The top layers were spin-coated onto mica using the spin speeds and solutions given in table S3. The batch A samples are a subset of the 'batch 1' samples presented in our study of equilibrated bilayers in Higgins et al[1] (batch A includes only 300k and 5k PS samples). The batch B samples were not presented or discussed in Higgins et al.

| **Batch A** | **Top layer solutions and spin speeds** |
|---|---|
| Sample A | 1.5 wt% 300k PS in toluene at 2.4k RPM |
| Sample B | " |
| Sample C | " |
| Sample D | 1.6 wt% solution (solutes; 34 wt% BisPCBM/66 wt% 300k PS) in chlorobenzene @ 2.5k RPM |
| Sample E | " |
| Sample F | 2 wt% 5k PS in toluene at 2k RPM |
| Sample G | 2.3 wt% solution (solutes; 33 wt% BisPCBM/67 wt% 5k PS) in chlorobenzene @ 3k RPM |
| **Batch B** | |
| Sample $\alpha$ | 1.5 wt% 300k PS in toluene @ 2.4k RPM |
| Sample $\beta$ | " |
| Sample $\gamma$ | " |

**Table S3; Solutions and spin speeds used in fabricating the top layers in batches A and B.**

The film floating process is represented schematically in figure S8_1. The substrate/bottom layer is placed just below the water surface in a bath of de-ionised water, at a slight angle to the horizontal. The floating process is then carefully controlled by floating the top layer onto the surface of the water until the film is held along one edge by the mica substrate. Slow lowering of the water level then deposits the top layer onto the substrate/bottom layer. This produces a very uniform bilayer across the 2" diameter sample. There are, of course, still microscopic defects, which can be either isolated (zero dimensional) defects or take the form of (one dimensional) line defects. As discussed in some of our previous publications utilising floated films,[1,7,8] such defects, which take up very little of the area of the samples, have no significant effect on the NR. Example images from bilayer samples and a Bis-PCBM single layer (after annealing), taken using atomic force microscopy (AFM) and optical microscopy, are shown in figure S9_1.

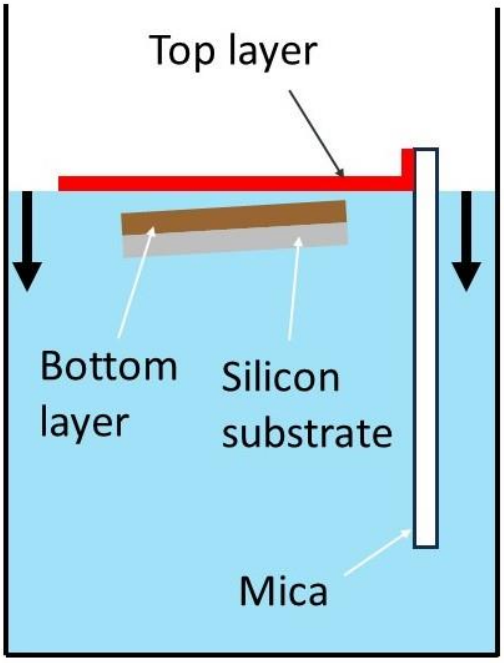


**Figure S8_1; A schematic diagram of the film floating methodology.**

## Thermal annealing and calibration; further details

The sample heater was placed within a vacuum chamber with quartz windows, that sits in the neutron beam. For all of the measurements on batch B (carried out on D17 in 2021), the windows were also covered with aluminium foil (NB; we neglected to include this detail in the supplementary information of Higgins et al[1]). Extensive calibrations were performed on duplicate silicon samples to establish the offsets between the controlling thermocouple within the heater block, and the sample surface temperatures, and the time taken for the sample temperature to stabilise following a temperature step. The data relating to these calibrations is shown in the supplementary information of Higgins et al.[1]

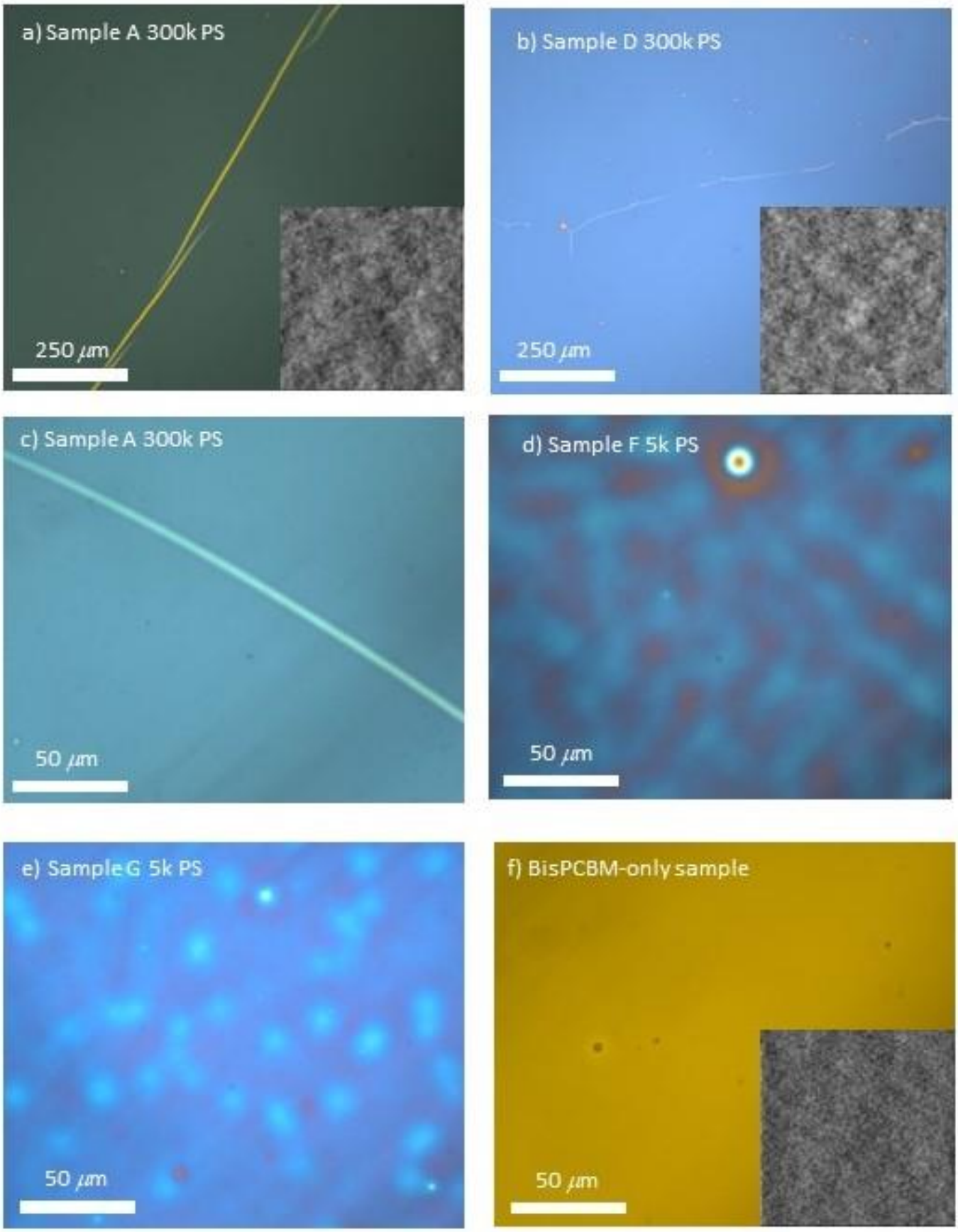


**Figure S9_1; Optical microscopy and AFM images from samples taken after annealing and cooling to room temperature.** a)-e) show optical micrographs of bilayer samples from batch A, after annealing on D17. f) shows an optical micrograph from a single Bis-PCBM layer sample, annealed on D17 along with the batch B samples (the NR from this sample is well-fitted by a single uniform layer, as-cast and during/thermal annealing; see figure S12 of Higgins et al[1] for fit parameters). The insets in a), b) and f) show 10 $\mu$m x 10 $\mu$m AFM images. The root-mean-square

roughnesses of the AFM images are all less than 1 nm. The images in a)-e) are specifically chosen to illustrate the kind of defects that occur during fabrication of bilayer samples.

### Data reduction; further details

The majority of samples were reduced using the standard 'incoherent' setting within Cosmos, which integrates specularly reflected neutrons from the detector map in a Cartesian fashion in scattering angle-wavelength ($\theta$–$\lambda$) space. One sample (sample F in batch A), which had broader specular reflections in the detector map was, however, reduced using the 'coherent' setting within Cosmos, which integrates within the specularly reflected region along contours of constant $q_z$ (momentum transfer in the direction normal to the sample). As discussed in Higgins et al,[1] these different methodologies gave very similar NR curves, fits, and extracted fit parameters.

### Data analysis; further details

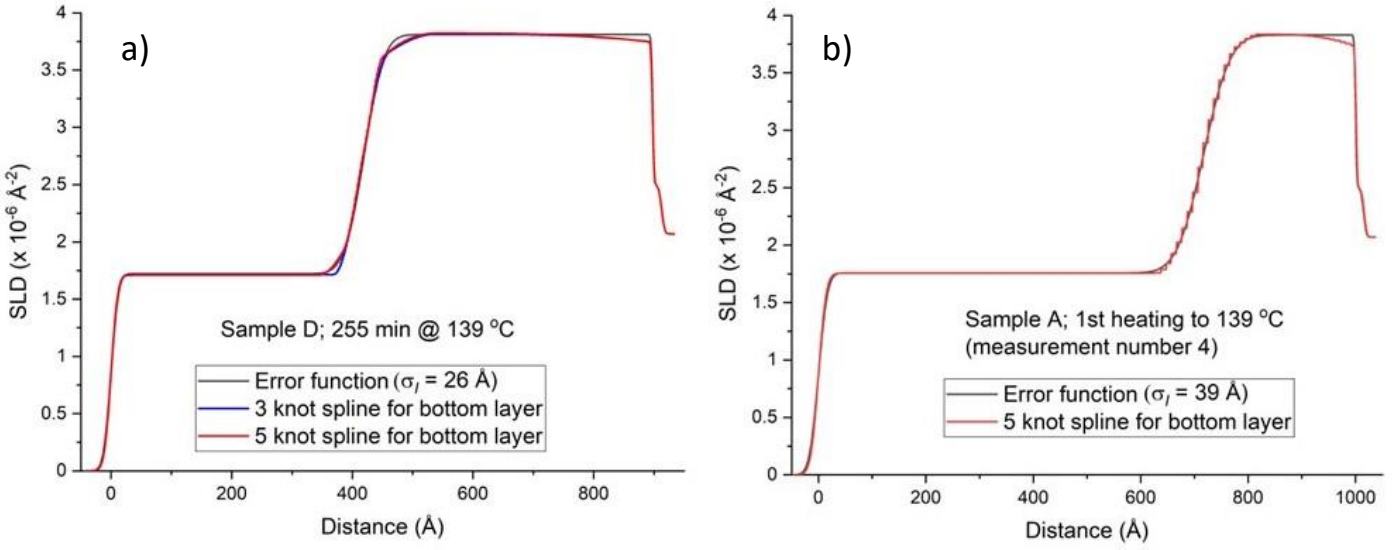


**Figure S10_1; Comparisons between error function bilayer fits (two uniform layers with Gaussian interfacial roughness) and free-form spline fits.** a) Sample D after 255 minutes at 139 °C, fitted with an error function profile (3 adjustable parameters for the bottom layer), and two different spline functions (one with 7 adjustable parameters for the bottom layer and one with 11 adjustable parameters for the bottom layer; the adjustable parameters are the layer thickness, plus the position and SLD of each knot).[9] b) Sample A on first heating to 139 °C, fitted with an error function profile and a 5-knot spline. For a), the goodness-of-fit, $\chi^2$, parameter was 327, 297 and 270 for the error function, 3-knot spline and 5-knot spline fits, respectively (for 246 data points). For b), $\chi^2$ was 300 and 284 for the error function and 5-knot spline fits, respectively (for 248 data points in the NR curve). NB in a) and b) the parameter 'microslab_max thickness'[9] was 2 Å and 10 Å respectively.

Constrained fits were performed using jupyter notebooks, with Levenburg-Marquardt and differential evolution algorithms. An example notebook can be found in the electronic supporting information. MCMC fits were also performed on selected NR curves for samples A, E, F and G (using the refnx GUI).[9] MCMC fits were typically performed with 200 walkers, 2000 steps, 'thin'=1 and 'temp'=-1. MCMC outputs for such a fit are shown in figures S11_1 to S11_3 for sample A. As well as the adjustable material parameters (SLD, layer thickness and roughness), the overall normalisation was allowed to vary slightly. This normalisation was carried out using refnx, rather than Cosmos; for all samples the normalisation factor, required to ensure that the reflectivity was equal to one below the critical angle, was around six. MCMC fits on were also performed with 200 walkers, 200 steps, 'thin'=250 and 'temp'=-1. Apart from the x-axis scale, the MCMC outputs for such a fit are almost identical to those shown in figures S11_1 to S11_3 (except for the slightly different autocorrelation plot, which is shown in figure S11_4). The median fit parameters and their

uncertainties, given in table S4, are also virtually identical for the two different MCMC fits (with different numbers of steps and different 'thin' parameters), illustrating the robustness of the methodology.

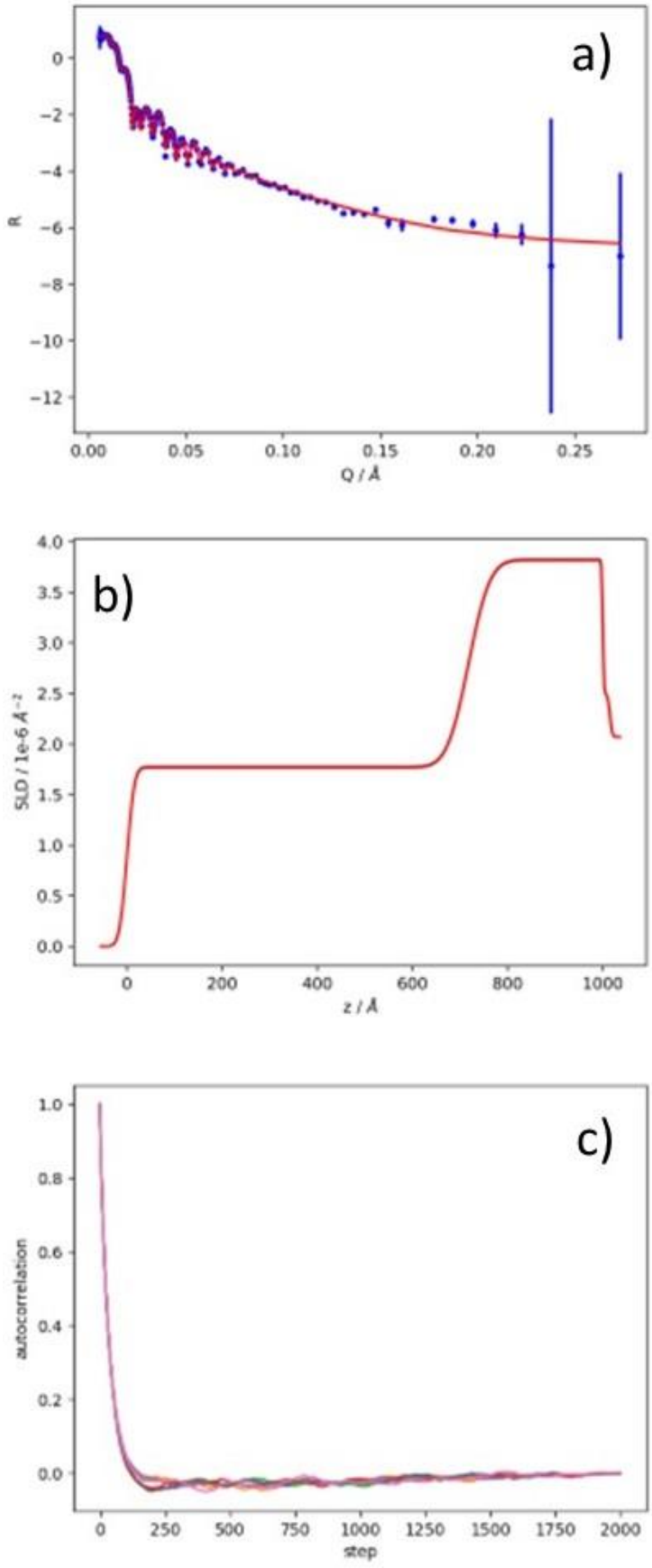


**Figure S11_1; MCMC fits for a typical NR measurement on sample A (run numbers 644027 and 644028; this is the first NR measurement at a sample surface temperature of 139 °C – see figures 4a and S4_1).** This run had 2000 steps, 200 walkers and 'thin'=1. a) Reflectivity, R, versus momentum transfer, Q. b) SLD versus distance, c) Autocorrelation of the 7 adjustable parameters (the 6 sample parameters, plus the normalisation of the R scale).[9]

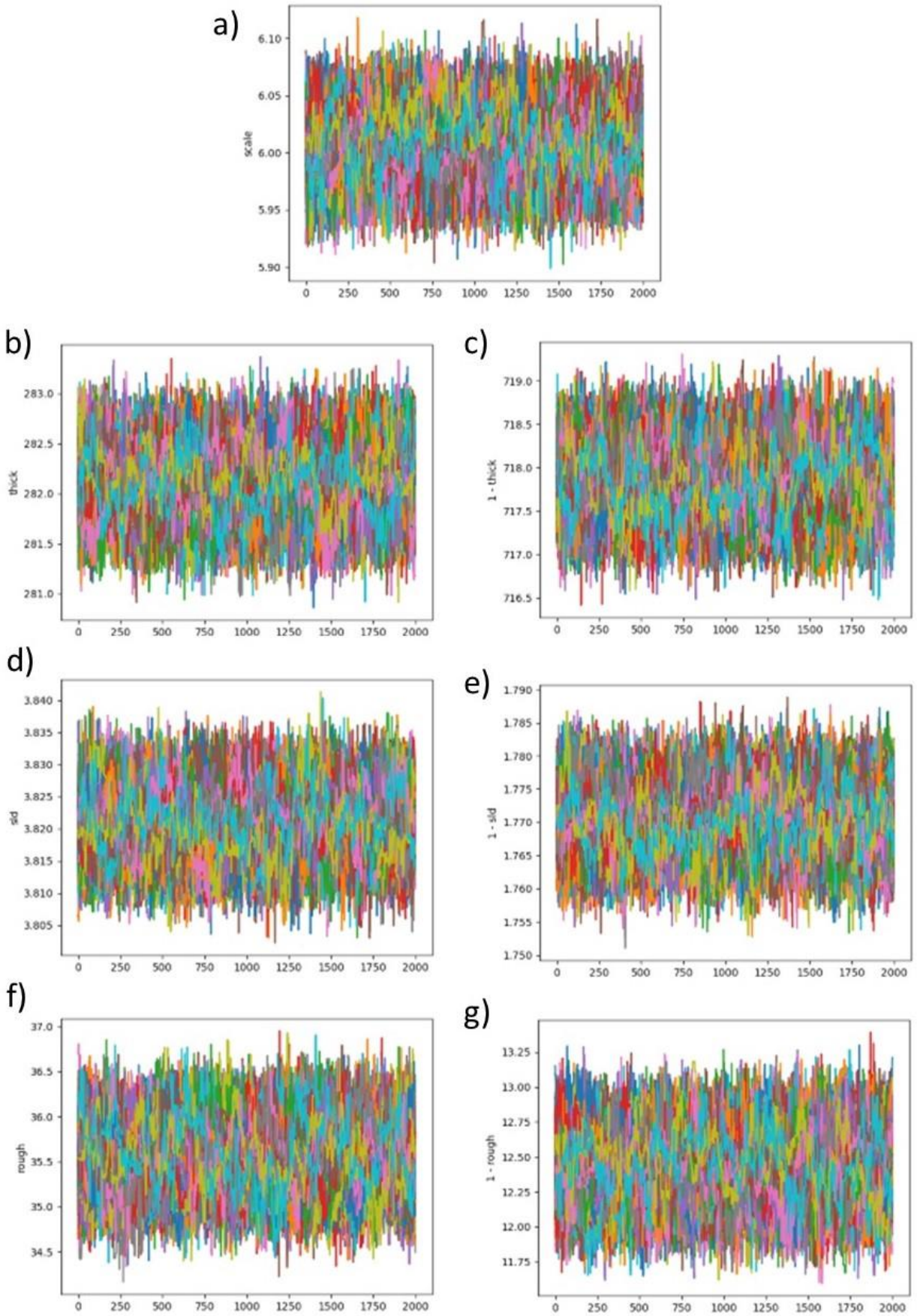


**Figure S11_2; MCMC fits for a typical NR measurement on sample A (run numbers 644027 and 644028; this is the first NR measurement at a sample surface temperature of 139 °C – see figures 4a and S4_1).** This run had 2000 steps, 200 walkers and 'thin'=1. The different colours show the changes in each of the 7 adjustable parameters for individual walks throughout the 2000 steps.[9] The parameters are a) normalisation, b) bottom layer thickness, c) top layer thickness, d) bottom layer SLD, e) top layer SLD, f) buried interface and g) sample surface.

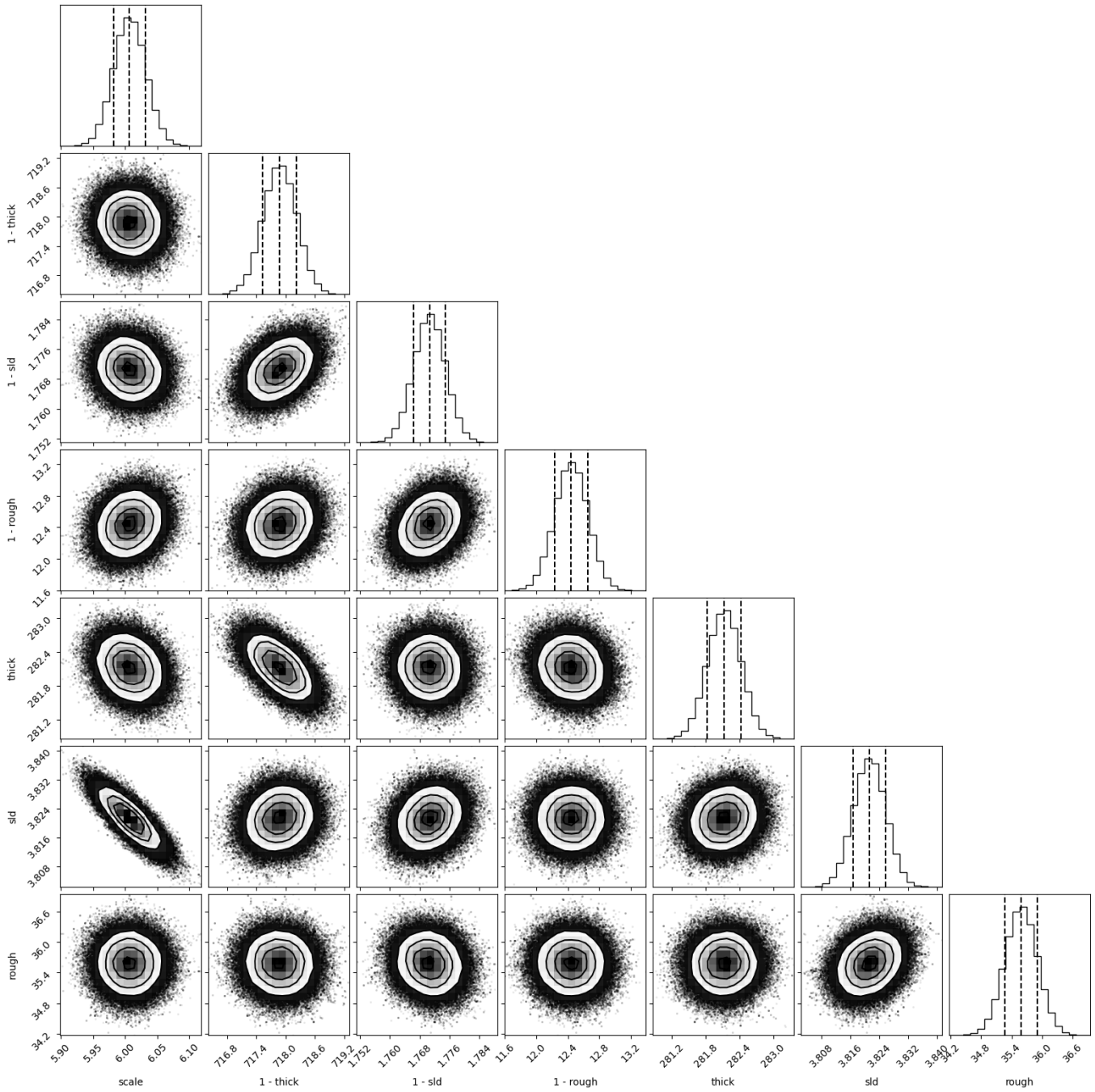


**Figure S11_3; MCMC fits for a typical NR measurement on sample A (run numbers 644027 and 644028; this is the first NR measurement at a sample surface temperature of 139 °C – see figures 4a and S4_1).** This run had 2000 steps, 200 walkers and 'thin'=1. Corner Plots.[9]

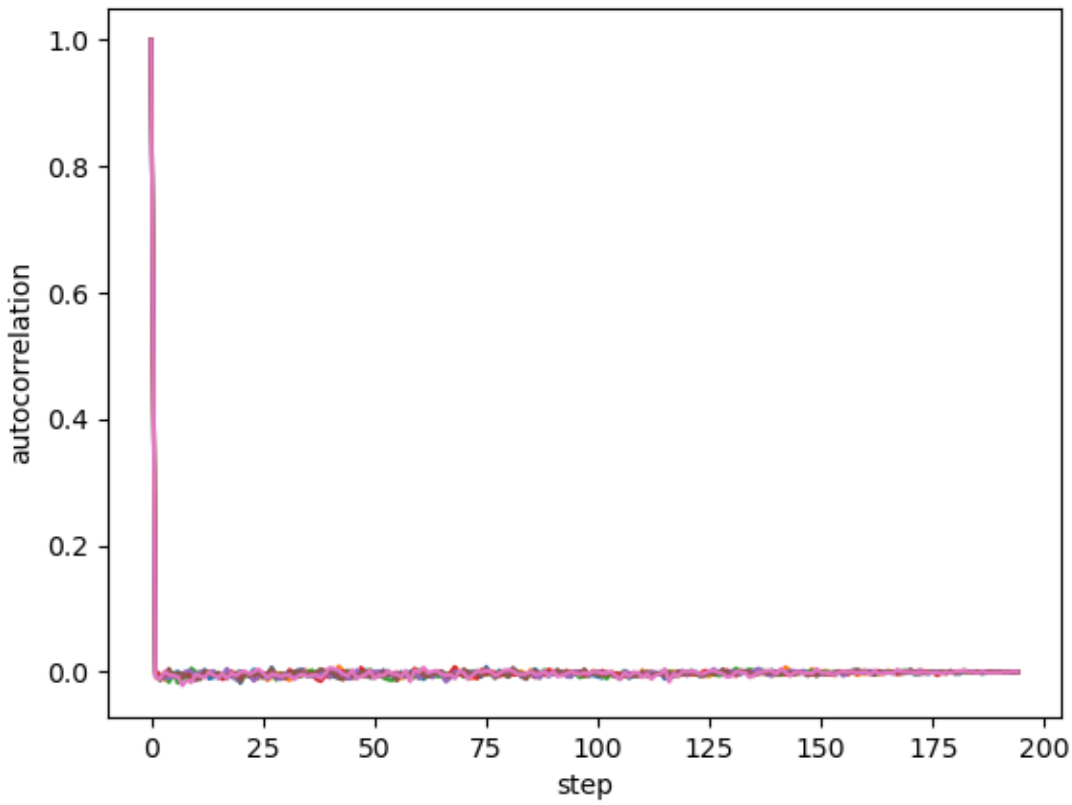


**Figure S11_4; MCMC fits for a typical NR measurement on sample A (run numbers 644027 and 644028; this is the first NR measurement at a sample surface temperature of 139 °C – see figures 4a and S4_1).** This run had 200 steps, 200 walkers, 'thin'=250and 'temp'=-1. Only the autocorrelation plot is shown here. The other plots are virtually identical to those shown in figures S11_1 to S11_3.

| | scale | $d_{top}$ | $\rho_{top}$ | $\sigma_s$ | $d_{bottom}$ | $\rho_{bottom}$ | $\sigma_I$ |
|---|---|---|---|---|---|---|---|
| 2000 steps, 'thin'= 1 | 6.007±0.025 | 717.9±0.35 | 1.77±0.0043 | 12.44±0.21 | 282.1±0.30 | 3.821±0.0045 | 35.59±0.32 |
| 200 steps, 'thin' = 250 | 6.007±0.025 | 717.9±0.34 | 1.77±0.0043 | 12.44±0.21 | 282.1±0.29 | 3.821±0.0045 | 35.59±0.32 |

**Table S4; Median fit parameters and uncertainties (approximately one standard deviation[9]) from the MCMC fits shown in figures S11_1 to S11_4.**

## Safety and hazards

**Chemicals and materials;** Material safety data sheets detailing hazards can be found for acetone, isopropanol, toluene and chlorobenzene on supplier websites, such as Sigma-Aldrich, Merck and Fisher Scientific. Material safety data sheets detailing hazards can be found for fullerenes on supplier websites, such as Solenne or Ossila.

**Sample fabrication**; The main hazards during sample fabrication are the use of chemicals, the use of a sharp (scalpel) blade to cleave the mica, and the high speed rotation of the spin-coater chuck/sample. Spin-coating of polymer and fullerene solutions should be carried out following a risk assessment. In this work this resulted in the use of a ballistic screen around the spin coater (which was placed in a well-ventilated space), and the use of appropriate personal protective equipment (lab coat, gloves and eye protection).

**Neutron reflectivity;** Appropriate training (including hazard identification) will be given by the central facilities, such as the Institut Laue-Langevin, prior to performing any neutron scattering experiments

## References for the Supporting Information


1 Higgins, A. M., Gutfreund, P., Italia, V. & Hynes, E. L. Equilibration and thermal reversibility in mixtures of model OPV small-molecules and polymers. *Journal of Materials Chemistry C* **11**, 2107-2119, doi:10.1039/d2tc04916c (2023).

2 James, D. *et al.* Measurement of molecular mixing at a conjugated polymer interface by specular and off-specular neutron scattering. *Soft matter* **11**, 9393-9403, doi:10.1039/c5sm02008e (2015).

3 Sferrazza, M. *et al.* Evidence for capillary waves at immiscible polymer/polymer interfaces. *Physical review letters* **78**, 3693-3696, doi:10.1103/PhysRevLett.78.3693 (1997).

4 Buff, F. P., Lovett, R. A. & Stillinger, F. H. Interfacial density profile for fluids in the critical region. *Physical review letters* **15**, 621-623 (1965).

5 Rowlinson, J. S. & Widom, B. *Molecular Theory of Capiliarity*. (Oxford University Press, 1989).

6 Sinha, S. K., Sirota, E. B., Garoff, S. & Stanley, H. B. X-ray and Neutron-Scattering from Rough Surfaces. *Physical Review B* **38**, 2297-2311, doi:10.1103/PhysRevB.38.2297 (1988).

7 Hynes, E. L. *et al.* Interfacial width and phase equilibrium in polymer-fullerene thin-films. *Communications Physics* **2**, 112, doi:10.1038/s42005-019-0211-z (2019).

8 Môn, D. *et al.* Bimodal crystallization at polymer-fullerene interfaces. *Physical Chemistry Chemical Physics* **17**, 2216-2227, doi:10.1039/c4cp04253k (2015).

9 Nelson, A. R. J. & Prescott, S. W. refnx: neutron and X-ray reflectometry analysis in Python. *J Appl Crystallogr* **52**, 193-200, doi:10.1107/S1600576718017296 (2019).